Article

Phase stability and thermal expansion of ZnO solid solutions with 3d transition metal oxides synthesized at high pressure

Petr S. Sokolov,[1] ⓘ Andrey N. Baranov [2,] ⓘ and Vladimir L. Solozhenko[3] * ⓘ

[1] *National Research Centre "Kurchatov Institute" – IREA, 107076 Moscow, Russia*

[2] *Chemistry Department, Moscow State University, 119991 Moscow, Russia*

[3] *LSPM–CNRS, Université Sorbonne Paris Nord, 93430 Villetaneuse, France*

Abstract

Phase stability and thermal expansion of rock-salt $Me_{1-x}Zn_xO$ (Me = Ni^{2+}, Co^{2+}, Fe^{2+}, Mn^{2+}) solid solutions synthesized at high pressures and high temperatures have been studied by synchrotron X-ray diffraction in a wide ($0.1 \leq x \leq 0.8$) concentration range. At ambient pressure rs-$Me_{1-x}Zn_xO$ solid solutions were found kinetically stable up to 670-1100 K depending on the composition and type of Me^{2+} cation. Temperature-induced decomposition of the single-phase rock-salt solid solutions lead in most cases to the formation of a mixture of two solid solutions, with cubic and wurtzite structures. Oxidation of the Me^{2+} cation (Co, Mn) by atmospheric oxygen can result in formation of mixed higher oxides of these metals. In all the systems studied, the rock-salt solid solutions show a linear temperature dependence of the thermal expansion, but for the compositions with the highest ZnO content, deviations from the linear dependence are observed.

P.S. Sokolov (sokolov.petr@yandex.ru)

A.N. Baranov (anb@inorg.chem.msu.ru)

V.L. Solozhenko (vladimir.solozhenko@univ-paris13.fr)

---

* Corresponding author (e-mail: vladimir.solozhenko@univ-paris13.fr)

1. Introduction

At ambient conditions ZnO has hexagonal wurtzite (w) structure (space group $P6_3mc$) which transforms into cubic rock-salt (rs) structure (space group Fm-3m) at pressures above 6 GPa [1]. rs-ZnO and ZnO-based cubic solid solutions with different ions seem to be promising for optoelectronic and spintronics applications due to ability to incorporate much higher dopants' concentrations as compared with the wurtzite phase. The octahedral oxygen environment in rock-salt ZnO removes the crystallochemical limitations for the introduction of a variety of cations. Hence, the properties of the solid solution can be tuned over a wide range of dopant concentrations while remaining within the field of its phase stability. Examples of materials interesting from the point of view of their semiconducting properties are ZnO solid solutions with magnesium oxide [2,3] and nickel oxide [4,5]. The research is developing in two directions: epitaxial stabilization of rs-ZnO in thin films on oriented substrates [2-5] and high-pressure phase transition of wurtzite ZnO into cubic one [6-16].

At ambient pressure the solubility of Ni^{2+} in w-ZnO is extremely low, being 0.9 mol% at 1100 K. The solubility of Zn^{2+} in rs-NiO is much higher, namely, 29 mol% at 1100 K [17] or 35 mol% at ~1500 K [18]. At 1100 K, the solubility of Co^{2+} in w-ZnO is 6.5 mol% while Zn^{2+} solubility in rs-CoO is three times higher, reaching 22 mol% [17]. Equilibrium T-x phase diagram of the FeO-ZnO system was previously studied at ambient pressure [19]. Like other MeO-ZnO systems, this system is characterized by a large (18-80 mol% ZnO at 1100 K) area of co-existence of wurtzite and rock-salt solid solutions. At 0.1 GPa and 1100 K, the Mn^{2+} solubility in w-ZnO reaches 25 mol% [17], which is the highest solubility value of all 3d transition metal ions. At the same time, Zn^{2+} solubility in rs-MnO is not more than 9 mol%, which is the lowest solubility of Zn^{2+} among 3d transition metal monoxides with rock-salt structure [17].

The kinetic stabilization of metastable rs-ZnO at ambient pressure can be achieved by quenching of microcrystalline ZnO-based solid solutions with a relatively high (up to 80 mol%) ZnO content from high pressure and high temperature. Recently, metastable rs-Me$_{1-x}$Zn$_x$O (Me = Mg^{2+}, Ni^{2+}, Co^{2+}, Fe^{2+}, Mn^{2+}) solid solutions have been successfully synthesized by quenching from 4.6-7.7 GPa and 1450-1650 K in the wide concentration range [6,7,9-13]. It has been found that the widest ($x \leq 0.8$) compositional range for the existence of single-phase rock-salt solid solutions is observed for the NiO-ZnO system, due to smaller radii and the energetic preference of octahedral coordination over tetrahedral [9]. rs-Co$_{1-x}$Zn$_x$O, rs-Fe$_{1-x}$Zn$_x$O and rs-Mn$_{1-x}$Zn$_x$O solid solutions can only be quenched to ambient conditions with much lower ZnO content. However, the use of nanocrystalline w-ZnO allows single-phase rs-ZnO to be quenched from 7.7 GPa and 770-820 K [20-22].

Crystallographic features of the structure [14-16,21-24], functional properties [4,5,8,15,22] and thermal expansion [21,25,26] of simple and complex metastable oxide systems remain a subject of particular attention due to future prospects for their practical application. The presence of transition metals in zinc oxide makes it possible to tune the band gap of such solid solutions over a wide range

[4-6,8] and to significantly influence their transport and magnetic properties [4,5,15,18]. In this regard, it is necessary to know the thermal stability ranges of these solid solutions, and for the possibility of combining them with other materials, it is also crucial to know their thermal expansion coefficients. At the same time, systematic studies of thermal stability of metastable solid solutions depending on the nature of the substituent cations have not been performed, and such data are absent in the literature.

In the present work the phase stability and thermal expansion of a variety of metastable ZnO solid solutions with 3d transition metal oxides synthesized at high pressures and high temperatures have been studied.

2. Experimental

2.1. Sample preparation

As starting materials, high-purity powders of wurtzite ZnO (Alfa Aesar, 99.99%, 325 mesh), rock-salt CoO (Aldrich, 99.99%), MnO (Alfa Aesar, 99.99%, 325 mesh), NiO (Prolabo, 99%) and "FeO" (Aldrich, 99%, 10 mesh) have been used. The MeO-ZnO mixtures of various stoichiometries (ZnO molar fraction varied from 0.2 to 1.0 with 0.1 concentration step) were thoroughly ground in an agate mortar under acetone, then pressed into pellets and placed into gold capsules. High-pressure synthesis of solid solutions has been performed at 7.7 GPa and 1450-1650 K using a toroid-type high-pressure apparatus at LSPM-CNRS [9]. Experimental details have been described elsewhere [9,10]. Single-phase $rs\text{-}Co_{0.3}Zn_{0.7}O$, $rs\text{-}Co_{0.4}Zn_{0.6}O$ and $rs\text{-}Fe_{0.4}Zn_{0.6}O$ solid solutions have been synthesized by "sodium chloride matrix" method [10,11,20]. The mixture of oxides and NaCl (in weight ratio 1:5) has been treated at 7.7 GPa and 1500 K and subsequently quenched down to ambient conditions. The sodium chloride matrix was then carefully washed out with cold water.

The samples recovered from high-pressure experiments have been studied by powder X-ray diffraction (Equinox 1000 Inel diffractometer; Cu Kα and Co Kα radiation) and high resolution scanning electron microscopy (LEO Supra 50 VP, Karl Zeiss).

The recovered samples were either dark green (Ni^{2+}, Mn^{2+}, Co^{2+}) or almost black (Fe^{2+}), with the exception of pink $Co_{0.2}Zn_{0.8}O$ and $Co_{0.3}Zn_{0.7}O$. According to SEM data, all synthesized solid solutions were dense, virtually poreless ceramics with grain sizes ranging from 1 to 10 microns.

2.2. High-temperature X-ray diffraction measurements

Phase stability and thermal expansion of metastable $rs\text{-}Me_{1-x}Zn_xO$ solid solutions at ambient pressure have been studied by high-temperature synchrotron X-ray diffraction at the B2 powder diffraction beamline of the DORIS-III storage ring (HASYLAB-DESY). Debye-Scherrer geometry with rotating quartz capillary was used. The X-ray diffraction patterns were collected in the 10–70° 2θ-range (λ = 0.6515, 0.6874, 0.6876, 0.6882 Å in four independent experimental sessions) for

2 min in real time using the OBI image plate detector. A NIST powder LaB$_6$ (*Pm-3m*, $a = 4.15695$ Å) was used as standard sample for detector adjustment at 298 K. The furnace temperature was kept constant within 1 K using a Eurotherm temperature controller and Pt10%Rh– Pt thermocouple. The temperature calibration of the setup was performed using well-established reference points: CsCl solid state phase transition (*Pm-3m* → *Fm-3m*, 743 K), CsCl melting (919 K), KCl melting (1044 K) and NaCl melting (1074 K). Each following temperature point was set by increasing the heater power. The temperature step was 50 or 100 K. Before each data collection the sample temperature was stabilized for 2-3 min. The diffraction data were analyzed using DatLab software [27], and positions of diffraction lines were determined by fitting to the Pearson profile function. The lattice parameters were calculated by the least squares method.

3. Results and discussion

The ZnO-MeO solid solutions synthesized at high pressure and high temperature with subsequent quenching are kinetically stable under ambient conditions over a rather wide temperature range. In general, all metastable phases, including dense high-pressure phases, should undergo phase transformations into thermodynamically stable equilibrium phases. In the case of *rs*-Me$_{1-x}$Zn$_x$O solid solutions, we will deal not only with the rock-salt → wurtzite phase transitions, but also with the decomposition of supersaturated wurtzite solid solutions upon temperature increase. This decomposition can proceed by different mechanisms, including the stabilization of supersaturated solutions. The removal of existing kinetic barriers of phase transition/decomposition can be achieved by heating to high temperatures. The driving force for such processes is the difference in Gibbs free energy (Δ*G*) between high-pressure and low-pressure phases. The sign and magnitude of Δ*G* are determined primarily by the magnitude and sign of the difference in molar volumes of these phases.

3.1. NiO-ZnO system

Three rock-salt solid solutions (*rs*-Ni$_{1-x}$Zn$_x$O, x = 0.7; x = 0.8; x = 0.5) and initial NiO were selected for the high-temperature synchrotron X-ray diffraction study at ambient pressure. A representative sequence of powder diffraction patterns for the ultimate composition with the maximum ZnO content (Ni$_{0.2}$Zn$_{0.8}$O) collected during stepwise heating is shown in Fig. 1. At room temperature, only narrow intense symmetrical lines corresponding to the rock- salt (*Fm-3m*) phase are observed. The first signs of change become visible at 973 K, when weak and broad reflections of the wurtzite phase appear, indicating the beginning of the decomposition of the initial single-phase cubic solid solution into a mixture of two solid solutions according to the following scheme

$$rs\text{-Ni}_{1-x}\text{Zn}_x\text{O} \rightarrow rs\text{-Ni}_{1-y}\text{Zn}_y\text{O} + w\text{-Zn}_{1-z}\text{Ni}_z\text{O}$$
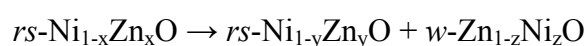
where x > y, *i.e.*, the cubic phase is depleted in zinc, whereas the wurtzite phase may be enriched with nickel to a much greater extent than the equilibrium value of 0.9 mol% [17], apparently due to the non-equilibrium conditions of its formation.

For the $Ni_{0.3}Zn_{0.7}O$ composition the onset temperature of cubic phase decomposition (T_d) is 1100 K (the highest temperature for the experimental setup used), and for *rs*-$Ni_{0.5}Zn_{0.5}O$ solid solution no changes were observed in the whole temperature range studied. Thus, *rs*-$Ni_{1-x}Zn_xO$ solid solutions exhibit high kinetic and phase stability, *i.e.*, up to $\sim\frac{1}{2}T_{melting}$, which is quite unique for metastable high-pressure phases. Previously, such high phase stability has only been observed for coesite and stishovite, high-pressure phases of SiO_2, which are kinetically stable up to 973-1073 K at ambient pressure [28-31].

It should be noted that, the main role in the stabilization of cubic ZnO-NiO solid solutions seems to be played by the small size of Ni^{2+} cation (0.69 Å *versus* 0.74 Å for Zn^{2+} [32]) and its strong preference for the octahedral environment in oxide compounds [33]. Another feature of nickel compared to other 3d transition metals is the high resistance to oxidation of the Ni^{2+} cation. In fact, oxidation to Ni^{3+} is only possible under rather harsher conditions, such as exposure to high-energy plasma [34], whereas bivalent cobalt, iron and manganese cations can be relatively easily oxidized to the +3 state by atmospheric oxygen upon heating. As will be shown below, oxidation can contribute to the thermal decomposition of cubic solid solutions with other 3d transition metals.

The temperature dependencies of the unit cell volumes of *rs*-$Ni_{1-x}Zn_xO$ solid solutions are presented in Fig. 2. The figure also shows the dependencies for pure nickel and zinc oxides. Experimental thermal expansion data were fitted to the following equation

$$V(T) = V_0[1 + \alpha_1(T-298) + \alpha_2(T-298)^2] \qquad (1)$$

the coefficients of which are given in Table 1. The unit for V(T) and V_0 is $Å^3$. Units for α_1 and α_2 are K^{-1} and K^{-2} respectively.
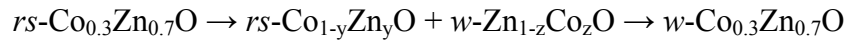
For nickel oxide, our data show an almost linear dependence close to the literature data [26]. At ambient pressure, metastable nanocrystalline rock-salt zinc oxide has a rather narrow temperature range of stability [20-22], and the scatter of the thermal expansion data is quite significant and determined by the chemical history of the precursor, *i.e.*, *w*-ZnO nanopowder [22]. Thus, in this case the powder microstructure - grain sizes, grain boundaries, etc. - make a significant contribution to the thermal expansion.

It should be noted that for the $Ni_{0.2}Zn_{0.8}O$, cubic solid solution with maximum ZnO content, the dependence V(T) is quadratic, whereas for the other compositions it is either linear or quasi-linear (Fig. 2, Table 1). The quadratic dependence V(T) has been previously observed for ZnO-rich cubic solid solutions in other systems [7,10,35,36]. In certain cases, non-linear thermal expansion in oxide systems has been attributed to phase heterogeneity, *i.e.*, the presence of foreign phases [25]. However, this is not the case here. According to the diffraction data, the samples were single-phase up to the appearance of wurtzite phase.

In fact, rs-Ni$_{1-x}$Zn$_x$O solid solutions show distinct structural features. As previously found by EXAFS spectroscopy, the Ni-O and Zn-O interatomic distances do not depend on the composition and are equal to r_{NiO}= 2.08 Å and r_{ZnO}= 2.14 Å, while the distances between the metal cations are not fixed [23,24]. X-ray diffraction methods are insensitive to this type of anomaly, and the latter can only be detected by local analysis methods. Consequently, if the increase in Ni-O and Zn-O distances during heating is linear, but each according to its own dependence, the overall change will already be non-linear. Moreover, this deviation from linearity should only occur for compositions with a high zinc oxide content, and may indicate that the solid solution concerned is nonequilibrium.
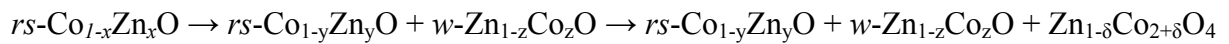
3.2. CoO-ZnO system

The phase stability and thermal expansion of rs-Co$_{1-x}$Zn$_x$O solid solutions at ambient pressure have been studied for seven compositions ($0.1 \leq x \leq 0.7$, in steps of 0.1). The sequence of powder X-ray diffraction patterns for the compositions Co$_{0.3}$Zn$_{0.7}$O and Co$_{0.4}$Zn$_{0.6}$O under stepwise heating is shown in Figs. 3a and 3b, respectively. At room temperature both samples are single-phase cubic. As the temperature increases, the full width at half maximum (FWHM) of the 200 line of the cubic phase remains almost constant up to the onset of the phase transition. For the rs-Co$_{0.3}$Zn$_{0.7}$O sample the first weak lines of the wurtzite phase appear at 573 K, the cubic phase remains present up to 873 K, and the transformation is complete at 973 K. Thus, the scheme of phase transitions for this composition can be described as follows:

$$rs\text{-Co}_{0.3}\text{Zn}_{0.7}\text{O} \rightarrow rs\text{-Co}_{1-y}\text{Zn}_y\text{O} + w\text{-Zn}_{1-z}\text{Co}_z\text{O} \rightarrow w\text{-Co}_{0.3}\text{Zn}_{0.7}\text{O}$$

It should be noted that earlier single-phase solid solutions with wurtzite structure enriched with cobalt up to 30 mol% were only prepared in the form of thin films [37]. Thus, at high pressures it is possible to produce wurtzite zinc oxide solid solutions that are significantly cobalt-saturated compared to conventional ceramic synthesis methods.

For the rs-Co$_{0.4}$Zn$_{0.6}$O composition a more complicated behavior was observed: the first lines of the wurtzite phase appeared at 773 K, and they coexist with lines of the cubic phase in a rather wide temperature range. At 873 K, additional weak lines appeared which can be correlated with the cubic (Fd-$3m$) spinel Zn$_{1-\delta}$Co$_{2+\delta}$O$_4$, apparently due to partial oxidation of the sample by air oxygen. Similar behavior – decomposition into a mixture of three phases – was observed for all compositions with lower ZnO content ($0.3 \leq x \leq 0.6$):

$$rs\text{-Co}_{1-x}\text{Zn}_x\text{O} \rightarrow rs\text{-Co}_{1-y}\text{Zn}_y\text{O} + w\text{-Zn}_{1-z}\text{Co}_z\text{O} \rightarrow rs\text{-Co}_{1-y}\text{Zn}_y\text{O} + w\text{-Zn}_{1-z}\text{Co}_z\text{O} + \text{Zn}_{1-\delta}\text{Co}_{2+\delta}\text{O}_4$$

The temperature dependencies of the unit cell volumes of rock-salt CoO-ZnO solid solutions are shown in Fig. 4 and Table 2. Note that for the ZnO-rich compositions (Co$_{0.3}$Zn$_{0.7}$O and Co$_{0.4}$Zn$_{0.6}$O) the V(T) dependence is essentially quadratic, whereas for the other compositions this dependence is either linear or quasilinear (Table 2). The dependence of the linear thermal expansion coefficients

on the composition for all solid solutions of the CoO-ZnO system is shown in Supplementary Material (Fig. S1). In the $0.2 \leq x \leq 1$ concentration range, this dependence can be considered linear.

3.3 MnO-ZnO system

The phase stability and thermal expansion of four cubic solid solutions $Mn_{1-x}Zn_xO$ ($0.1 \leq x \leq 0.4$, in steps of 0.1) have been investigated. The dependence of unit cell parameter on the composition is shown in Fig. 5. This dependence is almost linear and follows Vegard's law, as in the case of the NiO-ZnO system [9].

The onset temperature of decomposition of rs-$Mn_{1-x}Zn_xO$ solid solutions increases with decreasing ZnO content, $e.g.$ from 800(25) K for x = 0.4 to 850(25) K for x = 0.3 and 940(50) K for x = 0.2. Our $in\ situ$ data agree well with the results of previous $ex\ situ$ experiments [8], where the rs-$Mn_{1-x}Zn_xO$ phase was found to be stable up to 673 K (x = 0.5) and to 773 K (x = 0.3), and lines of the wurtzite phase appeared only at temperatures of 773 and 873 K, respectively.

The sequence of powder X-ray diffraction patterns for the $Mn_{0.6}Zn_{0.4}O$ solid solution taken during stepwise heating is shown in Fig. 6. At room temperature, only narrow, intense and symmetric lines corresponding to the cubic phase are observed. At higher temperatures, the intensities of diffraction lines of the rock-salt phase decrease drastically, while weak and broad reflections of the wurtzite phase appear, indicating the decomposition of the initial single-phase solid solution into a mixture of wurtzite and rock-salt solid solutions.

For compositions x = 0.1 and x = 0 (pure MnO), the cubic phase is stable up to 1050 K inclusive; no lines of wurtzite phase appear, and only weak lines of higher manganese oxides hausmannite-Mn_3O_4 ($I4_1/amd$) and ramsdellite-MnO_2 ($Pnma$) become visible.

X-ray diffraction patterns of samples recovered after high temperature experiments showed the following phases: (1) rs-MnO based solid solution with lattice parameter $a \approx 4.43$ Å (for comparison, for pure rs-MnO $a = 4.444$ Å), corresponding to a Zn^{2+} doping of 8-9 mol%; (2) w-ZnO based solid solution with lattice parameters $a = 3.28(1)$ Å and $c = 5.24(1)$ Å, which are larger than the lattice parameters of pure w-ZnO ($a = 3.24986$ Å, $c = 5.20662$ Å; PDF 36-1451), corresponding to Mn^{2+} doping of 30-35 mol% [38]. Note that the equilibrium solubility of Mn^{2+} in w-ZnO for this system is not more than 25% [17]. A higher value (up to 35 mol%) has so far only been observed for thin films [38]. Thus, as in the case of the CoO-ZnO system, heating of metastable cubic solid solutions results in formation of highly supersaturated Mn^{2+} solid solutions with wurtzite structure.

The phase composition of the decomposition products of cubic MnO-ZnO solid solutions is also affected by Mn^{2+} oxidation, which is accompanied by the formation of hausmannite-like $Zn_{1-\delta}Mn_{2+\delta}O_4$ and ramsdellite-like MnO_2 due to partial oxidation by air at high (1000-1100 K) temperatures.

The temperature dependencies of the unit cell volumes of rs-$Mn_{1-x}Zn_xO$ solid solutions are presented in Fig. 7. For the stoichiometries $0.2 \leq x \leq 0.4$, unit cell volumes change non-linearly with temperature. The corresponding coefficients α_1 and α_2 of Eq. (1) are given in Table 3. For the equilibrium cubic solid solution (x = 0.1), as well as for pure rs-MnO, a practically linear dependence V(T) is observed (coefficient α_2 is small), whereas for the metastable solid solutions (x = 0.2, 0.3, 0.4) this dependence is quadratic (coefficient α_2 is relatively large).

3.4. FeO-ZnO system

The phase stability and thermal expansion of six rs-$Fe_{1-x}Zn_xO$ ($0.1 \leq x \leq 0.6$, in steps of 0.1) solid solutions have been investigated.

It should be noted that the FeO-ZnO system is significantly different from the previously described systems. This is mainly due to the fact that FeO (wüstite) is a non-stoichiometric compound [39] and at ambient pressure is only stable above 873 K. At lower temperatures it must decompose to a mixture of Fe + Fe_3O_4 (magnetite) [40], which is, however, kinetically hindered. According to X-ray diffraction data, the initial "FeO" (Aldrich) sample is a mixture of 96 wt% rs-$Fe_{0.925}O$ (wüstite) with lattice parameter $a = 4.308(1)$ Å and 4 wt% α-Fe. After high pressure − high temperature treatment, the iron impurity dissolves to form cubic $Fe_{0.985}O$ with lattice parameter $a = 4.312(1)$ Å, which is in good agreement with literature data [39,40].

This peculiarity of iron monoxide affects the behavior of its metastable cubic solid solutions under heating. If the decomposition of rs-$Fe_{1-x}Zn_xO$ ($0.4 \leq x \leq 0.6$) solid solutions can be described by the same scheme as for the other systems considered above, $i.e.$, by the formation of two solid solutions (cubic and wurtzite) with the possible presence of a spinel phase due to oxidation (Fig. 8a), for compositions with high iron content ($0.1 \leq x \leq 0.3$) a weak 101 line of α-Fe appears in the range of 800-1000 K (Fig. 8b), which disappears at higher temperatures.

Due to such chemical processes occurring in non-stoichiometric iron oxide, the temperature dependence of the lattice parameter of rs-$Fe_{1-x}Zn_xO$ above 700 K has a rather complex character. In the 300-700 K range the V(T) dependence for the equilibrium composition $Fe_{0.9}Zn_{0.1}O$ is practically linear, while for the metastable $Fe_{0.5}Zn_{0.5}O$ solid solution it is apparently quadratic (Fig. 9).

3.5 Comparison of phase stability of cubic solid solutions for different systems

The concentration dependence of the decomposition temperature of metastable rs-$Me_{1-x}Zn_xO$ solid solutions (T_d vs x) at ambient pressure for all investigated systems is shown in Fig. 10. It is easy to see that the cubic solid solutions of the NiO-ZnO system have the highest phase stability, and they also have the widest range of concentration stability [9]. Second and third in terms of thermal stability are the cubic solid solutions of the CoO-ZnO and MnO-ZnO systems, respectively. Finally, the cubic solid solutions of the FeO-ZnO system have the lowest phase stability, probably due to the

ease of the redox disproportionation processes $(3\,Fe^{2+} \rightarrow 2\,Fe^{3+} + Fe^0)$ observed already at relatively low temperatures.

Another possible explanation for this order of thermal stability may be due to the relatively low melting temperature of "FeO" (~1640 K [41]), which is 400-600 degrees lower than the melting temperatures of other 3d transition metal monoxides. In general, the thermal stability threshold of the studied cubic solid solutions is close to the corresponding values for the previously studied related metastable compounds of the $ZnO\text{-}LiTiO_2$ and $ZnO\text{-}LiFeO_2$ systems [10,11,35].

At the same time, the indicated order of decomposition onset of metastable solid solutions with 3d transition metal cations correlates with the number of electrons on their outer electron shell. The most stable are solid solutions of the NiO-ZnO system, in which the Ni^{2+} cation has the most stable electronic configuration $[Ar]3d^8$ and, according to crystal field theory, the greatest energy preference for the octahedral environment of the O^{2-} anions.

4. Conclusions

Thus, rock salt $Me_{1-x}Zn_xO$ solid solutions (Me = Ni^{2+}, Co^{2+}, Fe^{2+}, Mn^{2+}) are kinetically stable at ambient pressure up to 670-1100 K depending on composition and type of Me^{2+} cation. With increasing temperature, the phase transformation of the single-phase cubic solid solution $Me_{1-x}Zn_xO$ leads in most cases to a mixture of two solid solutions with cubic and wurtzite structures. For some cubic solid solutions of the CoO-ZnO system, their decomposition can result in formation of a single-phase solid solution with a wurtzite structure. Oxidation of the Me^{2+} cation (Co, Mn) by atmospheric oxygen at high temperatures can lead to the formation of mixed higher oxides of these metals. In solid solutions with iron oxide, the formation of magnetite and alpha-iron phases is possible at temperatures of 800-1000 K. In all systems studied, cubic solid solutions with maximum zinc oxide content show a quadratic temperature dependence of thermal expansion.

Author Contributions

Conceptualization, V.L.S. and A.N.B.; methodology, A.N.B. and V.L.S.; investigation, P.S.S., A.N.B and V.L.S.; formal analysis, P.S.S. and A.N.B.; data curation, P.S.S., A.N.B and V.L.S.; validation, A.N.B. and V.L.S.; resources, V.L.S.; writing—original draft preparation, A.N.B. and P.S.S.; writing—review and editing, V.L.S.; visualization, P.S.S.; supervision, V.L.S. All authors have read and agreed to the published version of the manuscript.

References

1. C.H. Bates, W.B. White, R. Roy, New High-Pressure Polymorph of Zinc Oxide. Science 137 (1962) 993. https://doi.org/10.1126/science.137.3534.993.a

2. M. Kunisu, I. Tanaka, T. Yamamoto, T. Suga, T. Mizoguchi, The formation of a rock-salt type ZnO thin film by low-level alloying with MgO. J. Phys. Condens. Matter 16 (2004) 3801. https://doi.org/10.1088/0953-8984/16/21/028

3. C.-Y. James Lu, Y.-T. Tu, T. Yan, A. Trampert, L. Chang, K.H. Ploog, Growth and stability of rocksalt $Zn_{1-x}Mg_xO$ epilayers and ZnO/MgO superlattice on MgO (100) substrate by molecular beam epitaxy. J. Chem. Phys. 144 (2016) 214704. https://doi.org/10.1063/1.4950885

4. K.O. Egbo, T.C. Chibueze, A.T. Raji, C.E. Ekuma, C.P. Liu, K.M. Yu, Effects of acceptor doping and oxygen stoichiometry on the properties of sputter-deposited p-type rocksalt $Ni_xZn_{1-x}O$ ($0.3 \leq x \leq 1.0$) alloys. J. Alloys Compd. 905 (2022) 164224. https://doi.org/10.1016/j.jallcom.2022.164224

5. C.P. Liu, K.O. Egbo, C.Y. Ho, Y. Wang, C.K. Xu, K.M. Yu, Wide-Gap $Zn_{1-x}Ni_xO$ alloy: A transparent p-type oxide. Phys. Rev. Appl. 13 (2020) 024049. https://doi.org/10.1103/PhysRevApplied.13.024049

6. A.N. Baranov, V.L. Solozhenko, C. Chateau, G. Bocquillon, J.P. Petitet, G.N. Panin, T.W. Kang, R.V. Shpanchenko, E.V. Antipov, Y.J. Oh, Cubic $Mg_xZn_{1-x}O$ wide band gap solid solutions synthesized at high pressures. J. Phys. Cond. Matter 7 (2005) 3377–3384. https://doi.org/10.1088/0953-8984/17/21/030

7. V.L. Solozhenko, A.N. Baranov, V.Z. Turkevich, High-pressure formation of $Mg_xZn_{1-x}O$ solid solutions with rock salt structure. Solid State Commun. 138 (2006) 534–537. https://doi.org/10.1016/j.ssc.2006.04.005

8. V.S. Bhadram, Q. Cheng, C.K. Chan, Y. Liu, S. Lany, K. Landskron, T.A. Strobel, $Zn_xMn_{1-x}O$ solid solutions in the rocksalt structure: Optical, charge transport, and photoelectrochemical properties. ACS Appl. Energy Mater. 1 (2018) 260–266. https://doi.org/10.1021/acsaem.7b00084

9. A.N. Baranov, P.S. Sokolov, O.O. Kurakevich, V.A. Tafeenko, D. Trots, V.L. Solozhenko, Synthesis of rock-salt MeO–ZnO solid solutions (Me=Ni^{2+}, Co^{2+}, Fe^{2+}, Mn^{2+}) at high pressure and high temperature. High Press. Res. 28 (2008) 515–519. https://doi.org/10.1080/08957959.2010.521653

10. P.S. Sokolov, *The synthesis of cubic ZnO and its solid solutions at high pressures and high temperatures.* PhD Thesis, Univ. Paris 13 (2010).

11. A.N. Baranov, P.S. Sokolov, V.L. Solozhenko, ZnO under Pressure: From Nanoparticles to Single Crystals. Crystals 12 (2022) 774 https://doi.org/10.3390/cryst12050744

12. P.S. Sokolov, A.N. Baranov, C. Lathe, V.L. Solozhenko, High-pressure synthesis of FeO–ZnO solid solutions with rock salt structure: in situ X-ray diffraction studies. High Press. Res. 30 (2010) 39–43. https://doi.org/10.1080/08957950903550236

13. P.S. Sokolov, A.N. Baranov, C. Lathe, V.Z. Turkevich, V.L. Solozhenko, High-pressure synthesis of MnO–ZnO solid solutions with rock salt structure: in situ X-ray diffraction studies. High Press. Res. 31 (2011) 43–47. https://doi.org/10.1080/08957959.2010.521653

14. V.I. Maksimov, S.F. Dubinin, A.N. Baranov, V.I. Sokolov, P.S. Sokolov, V.D. Parkhomenko, Structural state of metastable cubic compounds $Ni_{1-x}Zn_xO$ ($0.6 \leq x \leq 0.99$). Phys. Met. Metallogr. 114 (2013) 734–740. https://doi.org/10.1134/S0031918X13060094

15. S.F. Dubinin, V.I. Maksimov, V.D. Parkhomenko, V.I. Sokolov, A.N. Baranov, P.S. Sokolov, Y.A. Dorofeev, Fine structure and magnetism of the cubic oxide compound $Ni_{0.3}Zn_{0.7}O$. Phys. Solid State 53 (2011) 1362–1366. https://doi.org/10.1134/S1063783411070092

16. S.I. Gurskiy, V.A. Tafeenko, A.N. Baranov, Use of integrated intensities of X-ray powder diffraction patterns of $Mg_{1-x}Zn_xO$ solid solutions for the quantitative determination of their composition. Russ. J. Inorg. Chem. 53 (2008) 111–116. https://doi.org/10.1134/S0036023608010154

17. C.H. Bates, W.B. White, R. Roy, The solubility of transition metal oxides in zinc oxide and the reflectance spectra of Mn^{2+} and Fe^{2+} in tetrahedral fields. J. Inorg. Nucl. Chem. 28 (1966) 397–405. https://doi.org/10.1016/0022-1902(66)80318-4

18. D.-S. Sinn, Electrical properties of p-NiOn-ZnO two-phase mixtures. Solid State Ionics 83 (1996) 333–348. https://doi.org/10.1016/0167-2738(96)00010-0

19. S.A. Degterov, A.D. Pelton, E. Jak, P.C. Hayes, Experimental study of phase equilibria and thermodynamic optimization of the Fe-Zn-O system. Metall. Mater. Trans. B 32 (2001) 643–657. https://doi.org/10.1007/s11663-001-0119-2

20. P.S. Sokolov, A.N. Baranov, Z.V. Dobrohotova, V.L. Solozhenko, Synthesis and thermal stability of cubic ZnO in the salt nanocomposites. Rus. Chem. Bull. 59 (2010) 325–328. https://doi.org/10.1007/s11172-010-0082-7

21. P.S. Sokolov, A.N. Baranov, A.M.T. Bell, V.L. Solozhenko, Low-temperature thermal expansion of rock-salt ZnO. Solid State Commun. 177 (**2014**) 65–67. https://doi.org/10.1016/j.ssc.2013.10.006

22. A.N. Baranov, P.S. Sokolov, V.A. Tafeenko, C. Lathe, Y.V. Zubavichus, A.A. Veligzhanin, M.V. Chukichev, V.L. Solozhenko, Nanocrystallinity as a route to metastable phases: Rock salt ZnO. Chem. Mater. 25 (2010) 1775–1782. https://doi.org/10.1021/cm400293j

23. Y.A. Babanov, D.A. Ponomarev, V.V. Ustinov, Visualization of the atomic structure of solid solutions with the NaCl structure. Phys. Solid State. 57 (2015) 717–721. https://doi.org/10.1134/S106378341504006X

24. Y.A. Babanov, D.A. Ponomarev, V.V. Ustinov, A.N. Baranov, Y.V. Zubavichus, Local atomic structure of solid solutions with overlapping shells by EXAFS: The regularization method. J. Electron Spectrosc. 211 (2016) 1–11. https://doi.org/10.1016/j.elspec.2016.03.003

25. C.M. Rost, D.L. Schmuckler, C. Bumgardner, S.B. Hoque, D.R. Diercks, J.T. Gaskins, J.P. Maria, G.L. Brennecka, X. Li, P.E. Hopkins, On the thermal and mechanical properties of $Mg_{0.2}Co_{0.2}Ni_{0.2}Cu_{0.2}Zn_{0.2}O$ across the high-entropy to entropy-stabilized transition. APL Materials. 10 (2022) 121108 https://doi.org/10.1063/5.0122775

26. D. Taylor, Thermal expansion data: I. Binary Oxides with Sodium Chloride and Wurtzite Structures, MO. *Transactions and journal of British Ceramic Society 83* (1984) 5–9.

27. K. Syassen, Computer code DATLAB 1.34 (Max Plank Institute, Stuttgart, Germany, 2003).

28. A. Navrotsky, M. Akaogi, The quartz-coesite-stishovite transformations: new calorimetric measurements and calculation of phase diagrams. Phys. Earth. Planet. In. 36 (1984) 124–134. https://doi.org/10.1016/0031-9201(84)90013-X

29. J.L. Holm, O.J. Kleppa, E.F. Westrum Jr., Thermodynamics of polymorphic transformations in silica. Thermal properties from 5 to 1070° K and pressure-temperature stability fields for coesite and stishovite. Geochim. Cosmochim. Ac. 31 (1967) 2289–2307. https://doi.org/10.1016/0016-7037(67)90003-8

30. B.J. Skinner, J.J. Fahey, Observations on the inversion of Stishovite to silica glass. J. Geophys. Res. 68 (1963) 5595–5604. https://doi.org/10.1029/JZ068i019p05595

31. H. Ito, K. Kawada, S. Akimoto, Thermal expansion of stishovite. Phys. Earth. Planet. In. 8 (1974) 277-281. https://doi.org/10.1016/0031-9201(74)90094-6

32. R.D. Shannon, Revised effective ionic radii and systematic studies of interatomic distances in halides and chalcogenides. *Acta Crystallogr. A32* (1976) 751–767. https://doi.org/10.1107/S0567739476001551

33. V.S. Urusov, Interaction of cation on octahedral and tetrahedral sites in simples spinels − A reply. Phys. Chem. Miner. *10* (1984) 194-195. https://doi.org/10.1007/BF00311478

34. B. Zhang, X. Shang, Z. Jiang, C. Song, T. Maiyalagan, Z.-J. Jiang, Atmospheric-Pressure Plasma Jet-Induced Ultrafast Construction of an Ultrathin Nonstoichiometric Nickel Oxide Layer with Mixed Ni^{3+}/Ni^{2+} Ions and Rich Oxygen Defects as an Efficient Electrocatalyst for Oxygen Evolution Reaction. ACS Appl. Energy Mater. 4 (2021) 5059–5069. https://doi.org/10.1021/acsaem.1c00623

35. P.S. Sokolov, A.N. Baranov, V.A. Tafeenko, V.L. Solozhenko, High pressure synthesis of $LiMeO_2$–ZnO (Me = Fe^{3+}, Ti^{3+}) solid solutions with a rock salt structure. *High Press. Res.* 31 (2011) 304–309. https://doi.org/10.1080/08957959.2011.560844

36. V.L. Solozhenko, O.O. Kurakevych, P.S. Sokolov, A.N. Baranov, Kinetics of the wurtzite to rock-salt phase transformation in ZnO at high pressure. J. Phys. Chem. A 115 (2011) 4354–4358. https://doi.org/10.1021/jp201544f

37. L.I. Burova, S.V. Samoilenkov, M. Fonin, E. Biegger, Yu. Dedkov, E.A. Ganshina, O.Yu. Gorbenko, U. Rudiger, A.R. Kaul, Room temperature ferromagnetic (Zn,Co)O epitaxial films obtained by low-temperature MOCVD process. Thin Solid Films 515 (2007) 8490–8494. https://doi.org/10.1016/j.tsf.2007.03.099

38. T. Fukumura, Z. Jin, A. Ohtomo, H. Koinuma, M. Kawasaki, An oxide-diluted magnetic semiconductor: Mn-doped ZnO. Appl. Phys. Lett. 75 (1999) 3366. https://doi.org/10.1063/1.125353

39. H. Fjellvag, F. Gronvold, S. Stolen, B. Hauback, On the Crystallographic and Magnetic Structures of Nearly Stoichiometric Iron Monoxide. J. Solid State Chem. 124 (1996) 52–57. https://doi.org/10.1006/jssc.1996.0206

40. Y.W. Fei, S.K. Saxena, A thermochemical data base for phase equilibria in the system Fe-Mg-Si-O at high pressure and temperature. Phys. Chem. Miner. 13 (1986) 311–324. https://doi.org/10.1007/BF00308348

41. M.S. Seehra, H.P.J. Wijn (1992) H.P.J. Wijn (ed.) SpringerMaterials Various Other Oxides · MO, TiO – FeO, Landolt-Börnstein - Group III Condensed Matter 27G, (Various Other Oxides) https://materials.springer.com/lb/docs/sm_lbs_978-3-540-46749-6_3 (accessed on 14 March 2023).

Table 1   Parameters of Eq. (1) describing the thermal expansion data of rs-$Ni_{1-x}Zn_xO$ solid
solutions and NiO in the 300-1000 K temperature range

Composition, x	V_0 (Å^3)	$\alpha_1 \times 10^5$ (K^{-1})	$\alpha_2 \times 10^8$ (K^{-2})
0.8	77.42(1)	3.26(7)	2.34(13)
0.7	76.70(1)	4.00(10)	0.57(15)
0.5	75.63(2)	3.38(3)	—
(0) NiO	72.81(2)	4.34(3)	0.02(1)
(0) NiO*	73.29(2)	2.53(1)	1.29(1)

* 533-2200 K temperature range [26]

Table 2   Parameters of Eq. (1) describing the thermal expansion data of rs-$Co_{1-x}Zn_xO$ solid
solutions and CoO in the 300-900 K temperature range.

Composition, x	V_0 (Å^3)	$\alpha_1 \times 10^5$ (K^{-1})	$\alpha_2 \times 10^8$ (K^{-2})
0.7	78.17(1)	3.3(2)	2.6(7)
0.6	78.08(1)	3.5(1)	2.1(2)
0.5	77.859(2)	4.47(8)	0
0.4	77.773(2)	3.73(2)	0.87(4)
0.3	77.677(3)	3.60(4)	0.93(6)
0.2	77.62(3)	3.59(3)	0.84(5)
0.1	77.45(2)	3.78(3)	0.62(6)
0 (CoO)	77.266(6)	3.39(6)	0.96(10)
0 (CoO)*	77.215(1)	3.60(1)	0.695(1)

* 296-1273 K temperature range [26]

Table 3 Parameters of Eq. (1) describing the thermal expansion data of rs-Mn$_{1-x}$Zn$_x$O solid solutions and MnO in the 300-1000 K temperature range.

Composition, x	V_0 (Å^3)	$\alpha_1 \times 10^5$ (K^{-1})	$\alpha_2 \times 10^8$ (K^{-2})
0.4	84.04(2)	3.16(2)	3.90(17)
0.3	84.94(2)	3.12(1)	3.36(16)
0.2	85.78(2)	2.75(7)	4.36(11)
0.1	86.75(2)	4.13(3)	0.42(4)
0 (MnO)	87.80(1)	3.99(1)	0.45(10)
0 (MnO)*	87.76(1)	3.93(1)	0.49(1)

* 273-1473 K temperature range [26].
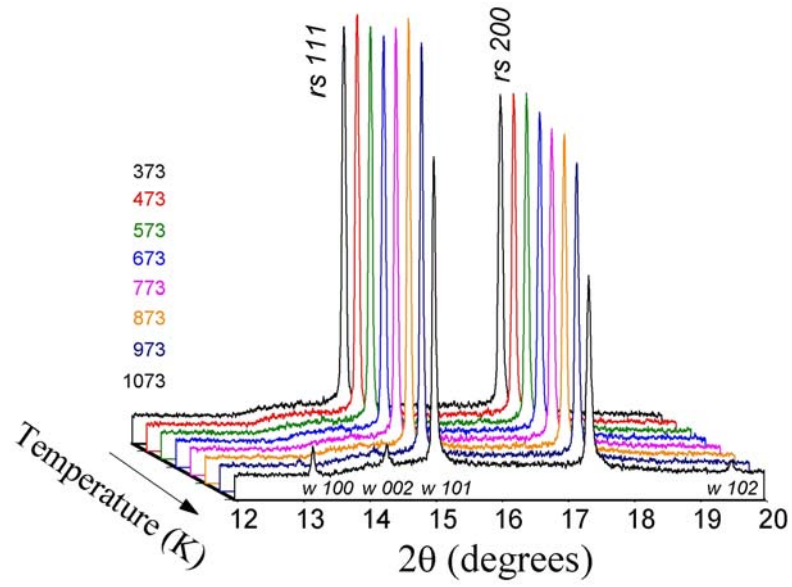
Fig. 1   Sequence of synchrotron powder X-ray diffraction patterns ($\lambda = 0.6515$ Å) of $Ni_{0.2}Zn_{0.8}O$ solid solution taken during stepwise heating to 1100 K. The rock-salt phase is stable up to ~970 K; the decomposition products are a mixture of two solid solutions, wurtzite and cubic.
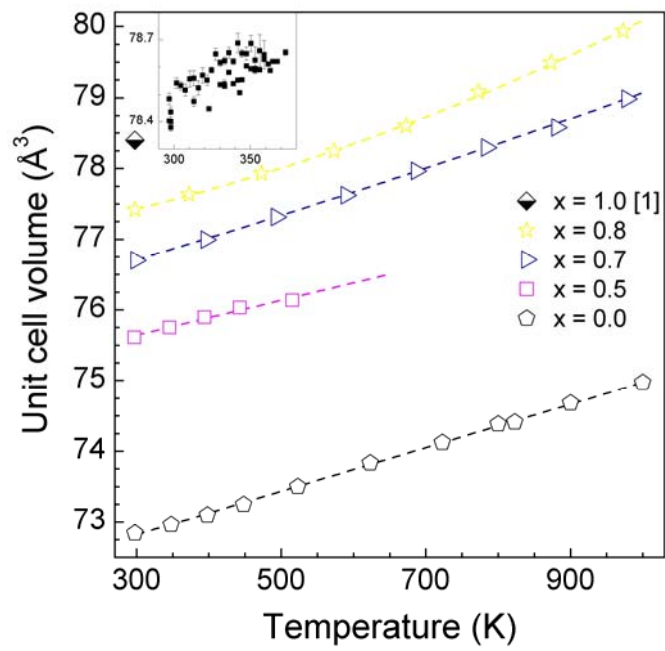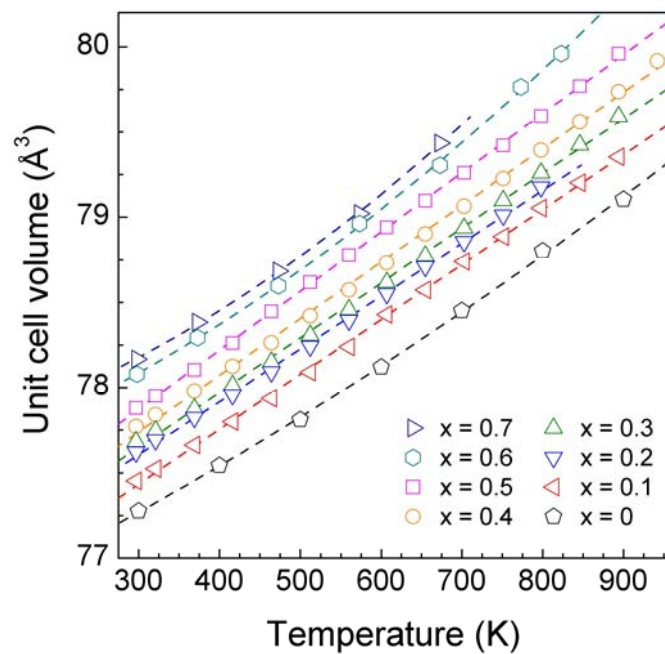
Fig. 2   Unit cell volumes of *rs*-Ni$_{1-x}$Zn$_x$O solid solutions *versus* temperature at ambient pressure. Error bars are smaller than the symbols. Dashed lines are least squares fits (see Table 1). Inset: small symbols correspond to our data on lattice parameters of nanocrystalline rock-salt ZnO in the 300-370 K range.
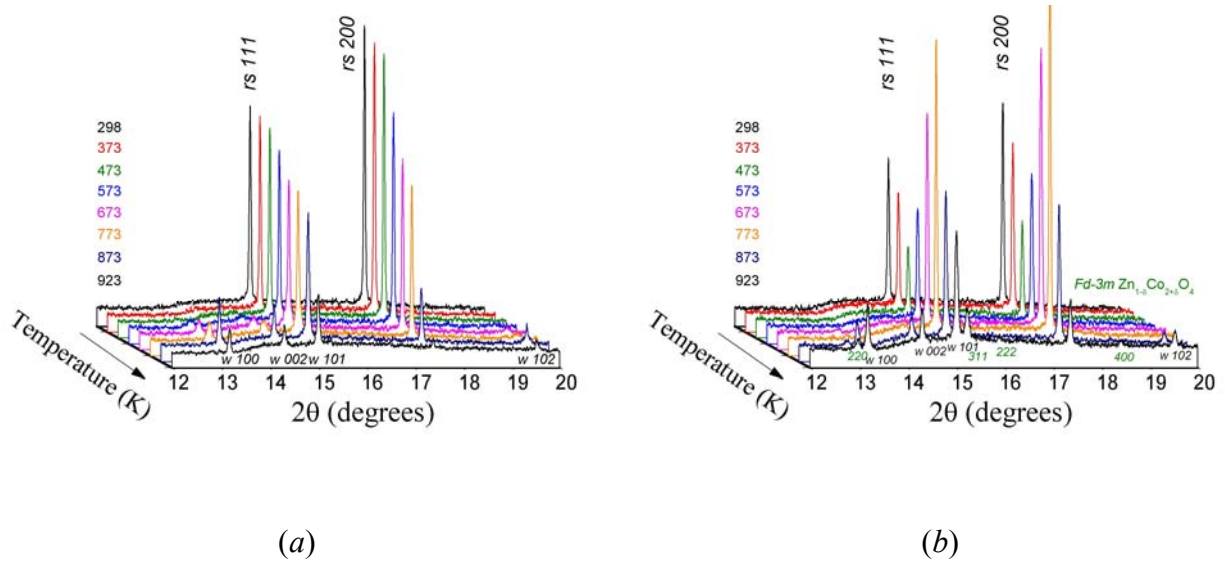
Fig. 3   Sequence of synchrotron powder X-ray diffraction patterns ($\lambda = 0.6515$ Å) of rock-salt $Co_{0.3}Zn_{0.7}O$ (*a*) and $Co_{0.4}Zn_{0.6}O$ (*b*) solid solutions taken during stepwise heating to 950 K. The first solid solution converts completely to a wurtzite structure, while the decomposition products of the second are a mixture of three phases - wurtzite, cubic and spinel-like.

Fig. 4   Unit cell volumes of *rs*-Co$_{1-x}$Zn$_x$O solid solutions *versus* temperature at ambient pressure. Error bars are smaller than the symbols. Dashed lines are least squares fits (see Table 2).
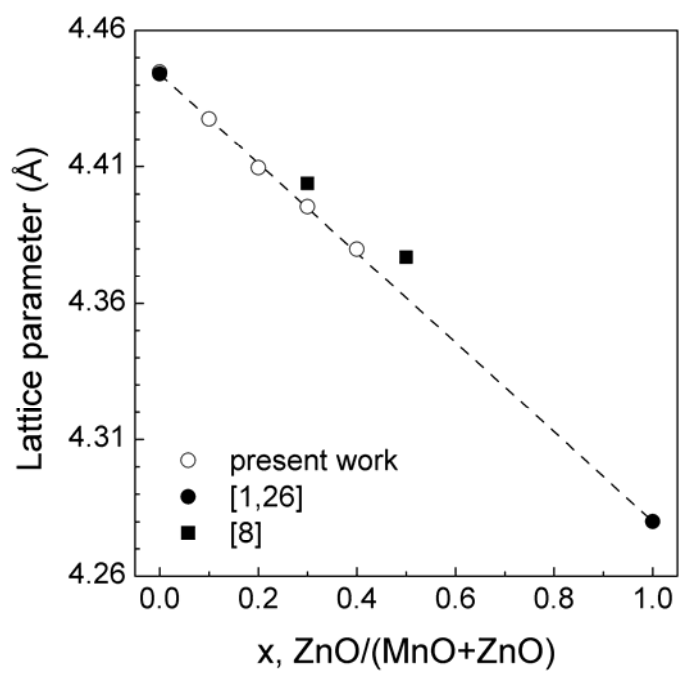
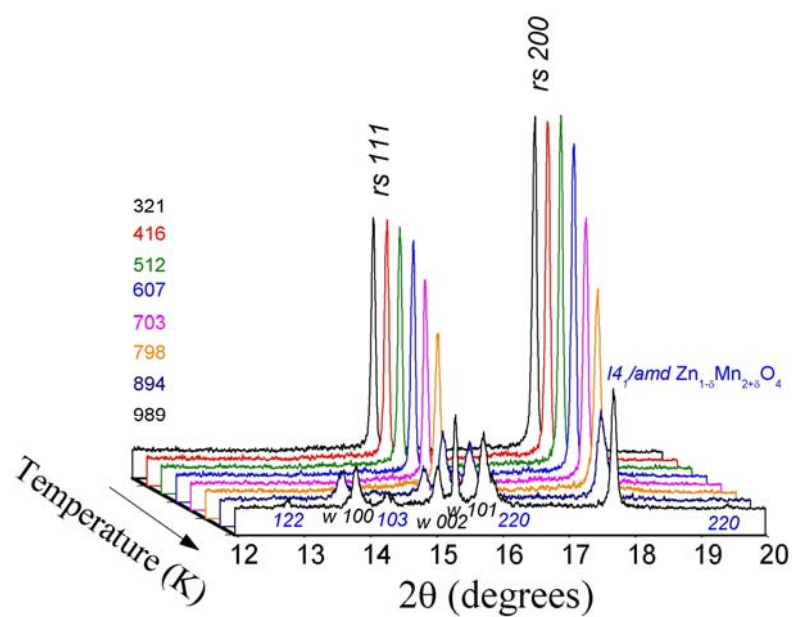Fig. 5 Lattice parameters of rs-Mn$_{1-x}$Zn$_x$O solid solutions as a function of composition.

Fig. 6   Sequence of synchrotron powder X-ray diffraction patterns ($\lambda = 0.6882$ Å) of $Mn_{0.6}Zn_{0.4}O$ solid solution taken during stepwise heating to 1000 K. The initial rock-salt phase is stable up to 850 K; the decomposition products are a mixture of three phases - wurtzite, cubic and spinel-like.
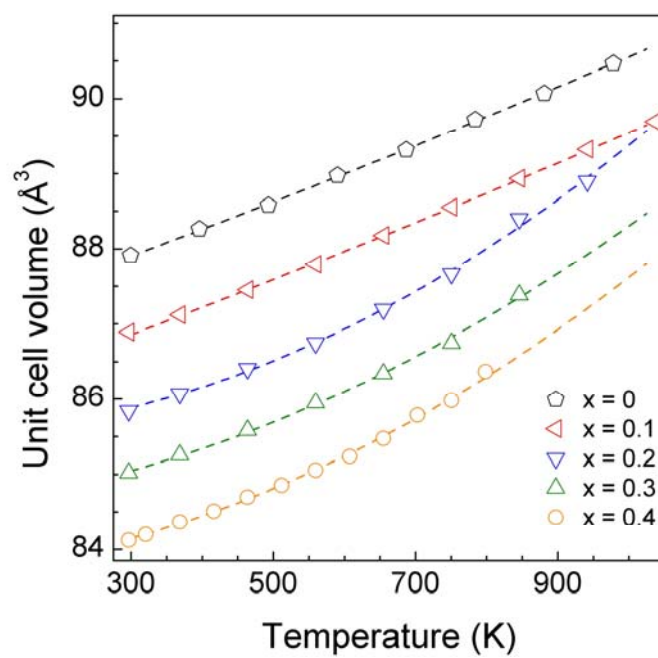
Fig. 7   Unit cell volumes of *rs*-Mn$_{1-x}$Zn$_x$O solid solutions *versus* temperature at ambient pressure. Error bars are smaller than the symbols. Dashed lines are least squares fits (see Table 3).
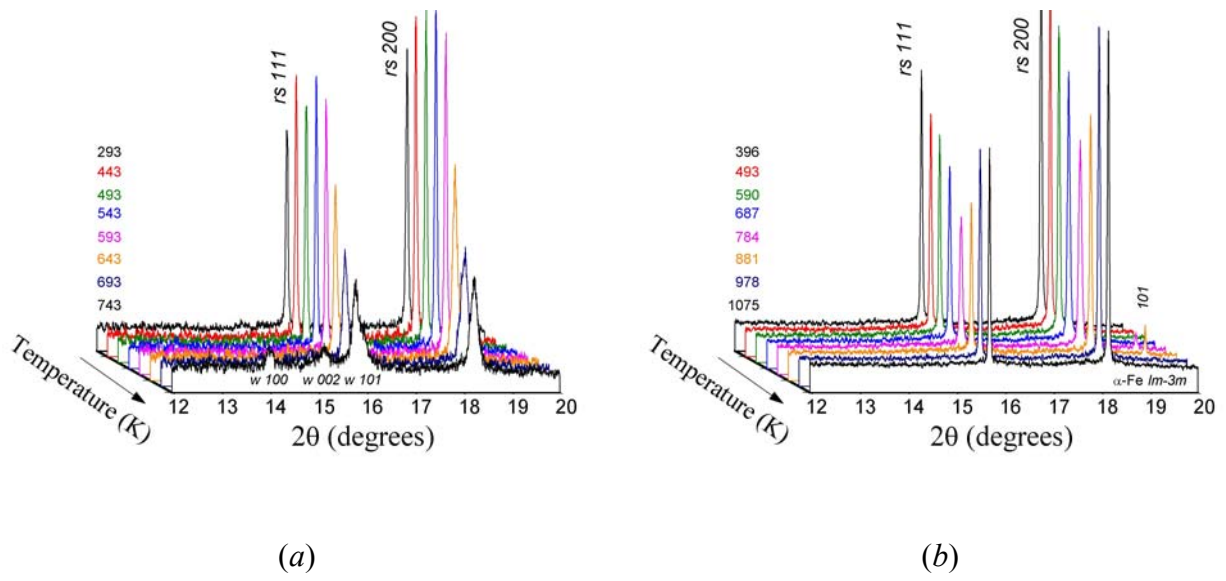
Fig. 8   Sequence of synchrotron powder X-ray diffraction patterns of rock-salt $Fe_{0.5}Zn_{0.5}O$ ($\lambda = 0.6876$ Å) (*a*) and $Fe_{0.9}Zn_{0.1}O$ ($\lambda = 0.6876$ Å) (*b*) solid solutions taken during stepwise heating. The first solid solution decomposes into a mixture of two phases, wurtzite and cubic; while the cubic structure of the second one remains stable over the whole temperature range studied, however, at 780 K the most intense line *101* of α-Fe (*Im*-3*m*) appears, which then disappears at 880 K.
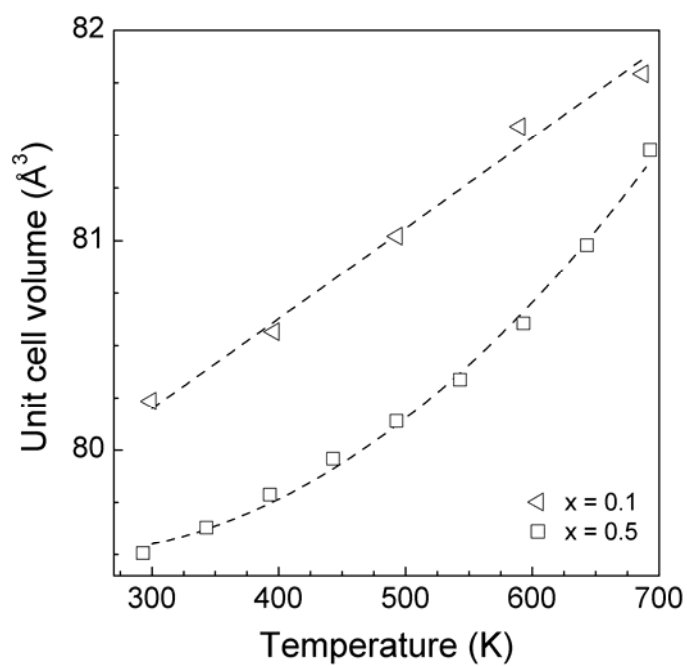
Fig. 9   Unit cell volumes of *rs*-Fe$_{1-x}$Zn$_x$O solid solutions *versus* temperature at ambient pressure. Error bars are smaller than the symbols. Dashed lines are just guides for the eye.
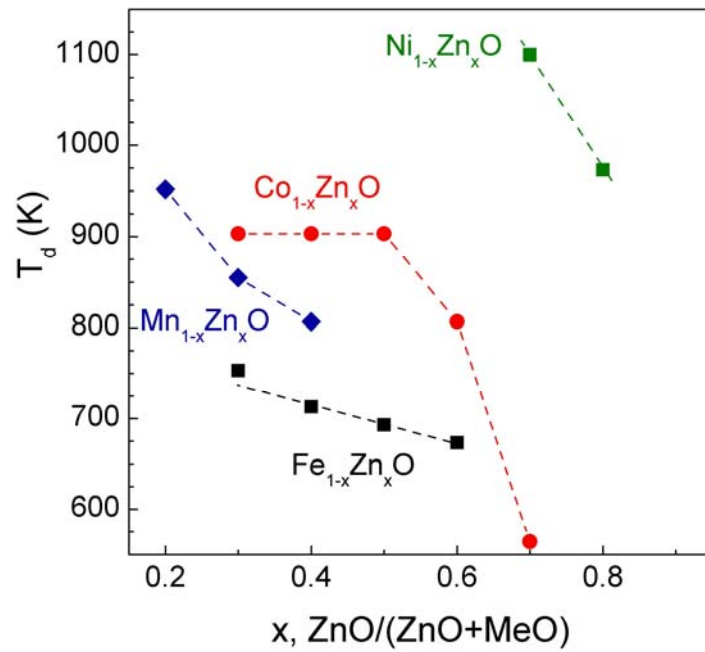
Fig. 10 Comparison of phase stability of rock-salt ZnO-MeO (Me = Ni, Co, Mn, Fe) solid solutions at ambient pressure. Below the dashed lines are the fields of kinetic stability of the corresponding cubic phases; above them the decomposition with formation of different phases is observed.